

Dynamical spin-triplet superconducting order induced by alternating electric fields

I. V. Bobkova,^{1,2,3} A. M. Bobkov,¹ and M.A. Silaev^{4,2,5}

¹*Institute of Solid State Physics, Chernogolovka, Moscow reg., 142432 Russia*

²*Moscow Institute of Physics and Technology, Dolgoprudny, 141700 Russia*

³*National Research University Higher School of Economics, Moscow, 101000 Russia*

⁴*Department of Physics and Nanoscience Center, University of Jyväskylä,
P.O. Box 35 (YFL), FI-40014 University of Jyväskylä, Finland*

⁵*Institute for Physics of Microstructures, Russian Academy of Sciences, 603950 Nizhny Novgorod, GSP-105, Russia*

(Dated: July 6, 2020)

Dynamical states offer extended possibilities to control the properties of quantum matter. Recent efforts are focused on studying the ordered states which appear exclusively under the time-dependent drives. Here we demonstrate a class of systems which feature dynamical spin-triplet superconducting order stimulated by the alternating electric field. The effect is based on the interplay of ferromagnetism, interfacial spin-orbital coupling and the oscillating motion of Cooper pairs. We demonstrate that the critical current of Josephson junctions hosting these states is proportional to the electromagnetic power, supplied either by the external irradiation or by the ac current source. Based on these unusual properties we propose the scheme of a Josephson transistor which can be switched by the ac voltage and demonstrates an even-numbered sequence of Shapiro steps. Combining the photo-active Josephson junctions with recently discovered Josephson phase batteries we find photo-magnetic SQUID devices which can generate spontaneous magnetic fields while being exposed to the irradiation.

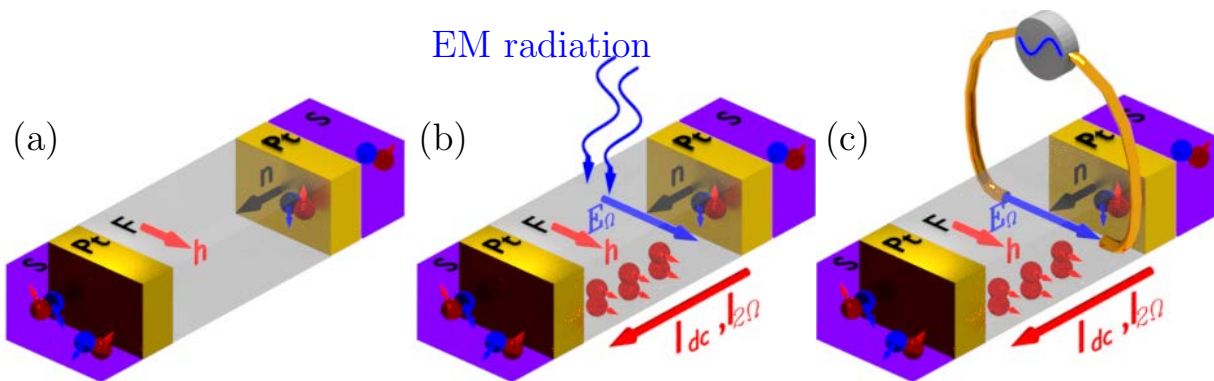


FIG. 1. **Schematic picture of the system considered.** S/F junction with Rashba SOC at the interface induced by the thin layer of heavy metal Pt. (a) Only short-range superconducting correlations are present shown by the blue and red spheres with opposite arrows. (b,c) generation of long-range triplet (LRT) correlations due to the irradiation of the setup with electromagnetic wave (b) and by applying the the ac current source (c) both producing the electric field $\mathbf{E}(t) = \mathbf{E}_0 e^{i\Omega t}$ in the ferromagnetic interlayer. The LRT are shown schematically by the red spheres with co-directed arrows corresponding to the spin states aligned with the exchange field \mathbf{h} . The LRT can transmit both the dc I_{dc} and the second harmonic $I_{2\Omega} e^{i\Omega t}$ Josephson currents between the superconducting electrodes.

I. INTRODUCTION

Weak links between two superconducting electrodes known as the Josephson junctions (JJ) are the cornerstone elements of superconducting electronics. For decades there has been an intensive search of technologies and physical principles allowing for the construction of superconducting transistors based on the JJ circuits with controllable switching between superconducting and resistive states¹. Such devices are expected to pave the way for energy-saving superconducting computers². Recently the interest to JJ with electrically-tunable critical currents has been stimulated by the perspectives of applying such systems in leading-edge quantum information architectures^{3,4}. Main efforts in this field has been focused on the systems with Josephson currents controlled by electrostatic gates. This concept has been realized in mesoscopic systems with normal metal interlayers^{5–10}, semiconducting interlayers^{1,3,4,11,12} and quantum dots^{13,14}. Electrostatic control with constant gate voltages is not enough for most of the applications imply transistors operating under the action of high-frequency drives. Therefore it is of crucial importance to go beyond the electrostatic gating and find the physical mechanisms which could provide control of the Josephson critical currents by the high-frequency electric field.

Here we suggest a qualitatively different way to controlling the Josephson current using dynamical superconducting states driven by the external time-dependent electric field. This mechanism can help to achieve switching rates in the terahertz and even the visible light frequency domains. It is based on the peculiar quantum state of matter which arises under the non-equilibrium conditions due to the interplay of Rashba-type^{15–17} interfacial spin-orbital coupling (SOC), ferromagnetism and oscillating motion of Cooper pairs driven by the alternating electric field. The proposed effect extends the possibilities of generating and controlling dynamical and non-equilibrium states of matter which has attracted significant attention recently. The prominent examples of such states include Floquet topological insulators¹⁸ time crystals^{19–21} driven Dirac materials²², light-induced superconductivity^{23,24} and dynamical hidden orders²⁵.

The prototype devices where our proposal can be realized are shown in Fig.1 where the SOC is introduced at the interfaces with the layers of a heavy metal such as Pt^{16,17}. The exchange field \mathbf{h} exists in the ferromagnetic (F) interlayer such as Ni, Co or Fe or even the half-metal CrO₂. Superconductivity is induced by the usual superconductors such as Al or Nb. The alternating electric field $\mathbf{E}(t)$ can be generated either by the electromagnetic (EM) radiation (blue wavy lines in 1b) or by the ac current source applied as shown in Fig.1c.

We demonstrate that the combination of these three key factors leads to the generation of the odd-frequency spin-triplet superconducting correlations which can penetrate into the ferromagnetic material over the large distances²⁶ Such correlations are shown schematically by the red circles with co-directed arrows in Fig.1b,c. In general, the spin-triplet Cooper pair is a coupled state of two electrons with the total spin equal to 1. Such a state can be formed by the superposition of three substates characterized by the different values of spin projection e.g. on the z axis: $|\uparrow\uparrow\rangle$ for $S_z = 1$, $|\downarrow\downarrow\rangle$ for $S_z = -1$ and $(|\uparrow\downarrow\rangle + |\downarrow\uparrow\rangle)$ for $S_z = 0$, where we use the usual intuitive notation for the spin-states of the two-electron system. Hence, the wave function of spin-triplet Cooper pairs or, more generally, the spin-triplet pairing amplitude can be written in terms of the spin vector²⁷ $\mathbf{d} = (d_x, d_y, d_z)$

$$\hat{f} = (d_x - id_y)|\uparrow\uparrow\rangle + (d_x + id_y)|\downarrow\downarrow\rangle + d_z(|\uparrow\downarrow\rangle + |\downarrow\uparrow\rangle) \quad (1)$$

Naturally such pairing is realized only in a few quite exotic systems like p-wave superfluid²⁷ ^3He . However it can be engineered in the designer hybrid systems consisting of ordinary superconductors and spin-textured ferromagnets^{26,28-31} or homogeneous ferromagnets with SOC³²⁻³⁶. Such systems can open great perspectives for low-dissipative spintronics^{37,38}. Recently they have attracted significant interest as a promising platform for realizing topological quantum devices^{39,40}.

Up to now the control of spin-triplet superconductivity has been considered mostly with the help of static fields while several works have studied the effect of magnetization procession on the Josephson current^{41?-44}. In this paper we demonstrate using the microscopic model of the diffusive ferromagnet and interfacial SOC that external time-dependent electric field produces triplet correlations with the spin vector constructed as follows

$$\mathbf{d}(\varepsilon, t) = \int dt' K_d(\varepsilon, t - t') (\mathbf{E}(t') \times \mathbf{n}) \times \mathbf{h}, \quad (2)$$

where \mathbf{n} is a normal to the interface plane with Rashba SOC. As usual, the spin vector \mathbf{d} depends on the quasiparticle energy ε . However, the problem under consideration is essentially non-stationary and for this reason it also depends on time. The scalar kernel $K_d(\varepsilon, t - t')$ is determined by the details of the microscopic model. The non-locality in time is determined by the characteristic frequencies of the superconducting condensate response to the alternating fields.

The order parameter (2) is an example of the recently proposed dynamical orders^{25,45-47}. It represents the state of matter which appears only under the non-equilibrium conditions determined by the alternating electric field. In contrast to the known systems with intrinsic spin-triplet pairing such as superfluid²⁷ He^3 the correlations given by Eqs. (1,2) correspond to the s-wave pairing because the spin vector in Eq. (2) does not depend on the direction of motion of the interacting electrons. Therefore the spin-triplet correlations Eq. (1) are robust to the impurity scattering. Besides that they represent the instance of the celebrated odd-frequency spin-triplet pairing states⁴⁸ which have attracted continual interest for several decades^{26,45,49-53}.

Switching on the high-frequency electric field satisfying condition $\mathbf{E} \times (\mathbf{n} \times \mathbf{h}) \neq 0$ leads to the generation of superconducting correlations (1,2) characterized by the spin projections ± 1 on the direction of the exchange field. This shows up through the property of such pairs to be robust to the spin depairing. At the distances $x \gg \xi_F$ only such pairs can survive in the ferromagnet hence named long-range triplets (LRT). In the absence of the electric field only the short-range pairs are produced which are localized at the coherence length $\xi_F \sim 1$ nm near the superconducting electrodes as shown schematically in Fig.1. Therefore with providing the microscopic mechanism behind the phenomenological construction of the spin vector (2) we claim to find the mechanism of electrically stimulated spin-triplet superconductivity which can support the long-range Josephson current through thick F layer as shown in Fig.1b,c. We suggest that such system can be considered as the photo-active Josephson junction (JJ). This terminology means that the Josephson current is switched on by the alternating electric field originating e.g. from the external electromagnetic radiation, as in Fig.1b. Alternatively, one can induce the Josephson current by applying the ac source to the F interlayer as shown in Fig.1c. This setup can be considered as the Josephson transistor controlled by the high-frequency voltage source. Below we describe the microscopic mechanism both on the qualitative level and provide calculations in terms of the time-dependent formalism describing non-equilibrium superconductivity in diffusive proximity systems.

For the photo-active JJ driven by the harmonic electromagnetic wave we get the unusual current-phase relation with time-dependent critical current:

$$I(\chi, t) = [I_{dc}^c + I_{2\Omega}^c \cos(2\Omega t)] \sin \chi \quad (3)$$

where χ is the phase difference between the superconducting electrodes. Note that here both the dc and double-frequency current amplitudes are determined by the alternating electric field $I_{dc}^c \propto E_\Omega E_{-\Omega}$ and $I_{2\Omega}^c \propto E_\Omega^2$.

II. RESULTS

A. Phenomenological description of the dynamical spin-triplet order

The qualitative physics of the effect can be described as follows. The effect of SOC is known to dwell on the electron spin and Lorentz transformation between electric and magnetic fields in the moving coordinate frame. That is, electric

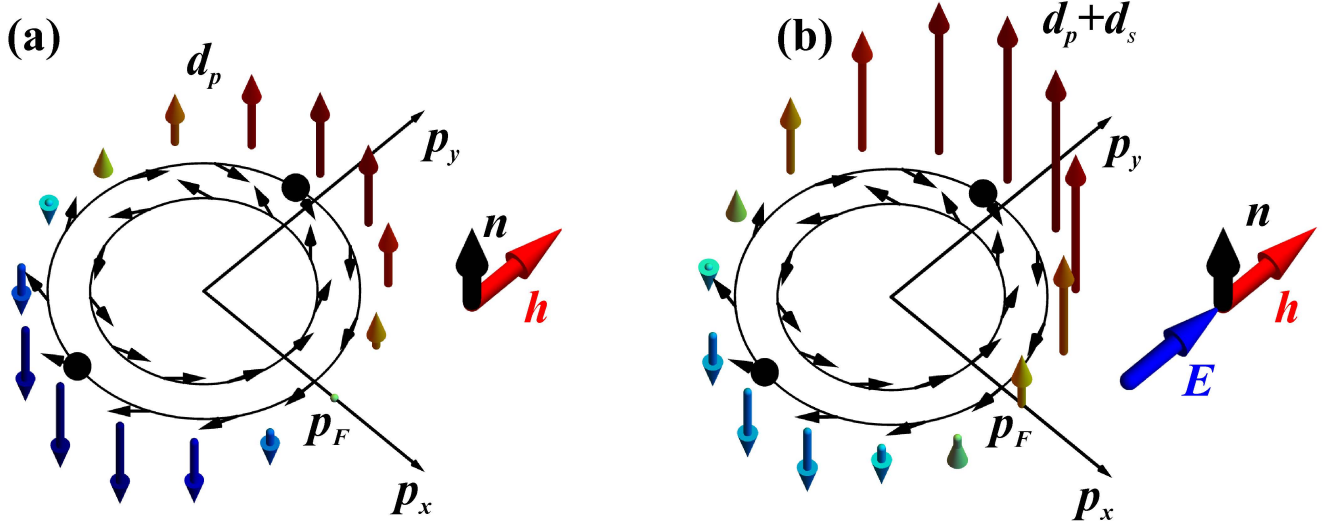


FIG. 2. Mechanism behind the formation of spin-triplet superconducting correlations. Ellipses show spin-split Fermi surface cross-sections in $p_x - p_y$ plane and small black arrows are the directions of spin quantization axes. Small black spheres show states with opposite momenta \mathbf{p} and $-\mathbf{p}$. Rashba SOC vector is $\mathbf{n} = \mathbf{z}$ and exchange field $\mathbf{h} = \hbar\mathbf{x}$. (a) Non-collinearity of spins at \mathbf{p} and $-\mathbf{p}$ results in the spin-triplet pairing with p-wave spin vector $\mathbf{d}_p \propto (\mathbf{n} \times \mathbf{p}) \times \mathbf{h} \parallel \mathbf{z}$. (b) Alternating electric field \mathbf{E} shown by the blue arrow results in the mixing between p and s-wave pairing amplitudes. This produces s-wave component of spin vector $\mathbf{d}_s \propto (\mathbf{n} \times \mathbf{E}) \times \mathbf{h}$ so that resulting vector $\mathbf{d} = \mathbf{d}_s + \mathbf{d}_p$ has non-zero average over the Fermi surface.

field \mathbf{E} , which is present in the laboratory frame, results in the magnetic field $\mathbf{B} = -\mathbf{v} \times \mathbf{E}/2c$ in the frame of the electron moving with the velocity \mathbf{v} . Acting on the electron spin this magnetic field induces the Zeeman shift of the energy which depends on the velocity \mathbf{v} . This fact makes drastic difference with the external magnetic field and prevents the electron ensemble to develop the net spin polarization in result of SOC. Consequently it greatly reduces the effect of SOC on spin-singlet Cooper pairs. Such pairs consist of electrons with opposite spins and momenta. Therefore SOC produces identical energy shifts for the interacting electrons and does not lead to the destruction of spin-singlet and, in general, opposite-spin Cooper pairs. This conclusion can be illustrated using the model of metallic system with Rashba-type SOC described by the Hamiltonian $\hat{H} = \xi_p + \alpha(\mathbf{p} \times \mathbf{n}) \cdot \boldsymbol{\sigma}$ where $\xi_p = p^2/2m - \varepsilon_F$ is the kinetic energy relative to the Fermi energy level ε_F . The presence of SOC in this Hamiltonian leads to the formation of helical bands. In these bands the spin quantization axes $\parallel (p_y, -p_x)$ rotate with changing of the position along the Fermi surface. However they still have collinear directions for the electron states with opposite momenta \mathbf{p} and $-\mathbf{p}$. Hence in this system superconducting state can be formed by the ordinary spin-singlet Cooper pairs provided that the spin splitting of Fermi surfaces is small, which is a typical situation for the interfacial SOC.

The situation changes drastically in the presence of external spin-splitting field, e.g. directed perpendicularly to the Rashba vector $\mathbf{h} = \hbar\mathbf{y}$. This field can be provided either by the Zeeman interaction with magnetic field or by the exchange interactions with adjacent ferromagnet as shown in Figs. 1. In this case the spin quantization axes are no longer collinear for the states with \mathbf{p} and $-\mathbf{p}$ as shown by the black spheres with arrows in Fig.2. Hence the pure spin-singlet pairing is no longer available. The interaction of electrons on the opposite sides of the Fermi surface leads to the formation of spin-triplet correlations characterized by the spin vector (1) which can be composed from the available fields as $\mathbf{d}_p(\mathbf{p}, \omega) = F_{pw}(\omega)\mathbf{h} \times (\mathbf{n} \times \mathbf{p})$ with the amplitude $F_{pw}(\omega)$ which is an even function of the Matsubara frequency ω . The typical texture of the spin vector is shown in Fig. 2. This state corresponds to the p-wave pairing because the order parameter is an odd function of momentum $\mathbf{d}_p(\mathbf{p}) = -\mathbf{d}_p(-\mathbf{p})$.

The external electric field producing oscillating motion of Cooper pairs is the third ingredient needed to produce the LRT. Indeed, the induced condensate motion with the condensate momentum $\mathbf{p}_s = -2ie\mathbf{E}\Omega/\Omega$ provides coupling between orbital p-wave and s-wave components.

The origin of this coupling can be understood considering the modification of quasiparticle spectrum by the added energy Doppler shift^{54,55} $\mathbf{v}_F \cdot \mathbf{p}_s$. Simultaneously this leads to the shift of imaginary frequencies so that the amplitude of triplet correlations is given by $F_{pw}(\omega - i\mathbf{v}_F \cdot \mathbf{p}_s) \approx F_{pw}(\omega) - i(\mathbf{v}_F \cdot \mathbf{p}_s)\partial_\omega F_{pw}$. This modification of the pairing amplitude produced the additional s-wave component the spin vector $\mathbf{d}_s = \langle \mathbf{d}_p(\mathbf{p}, \omega - i\mathbf{v}_F \mathbf{p}_s) \rangle$ where angular brackets denote averaging over the Fermi momentum directions. As a result we obtain the expression for the s-wave amplitude $\mathbf{d}_s = (2/3i)E_F(\partial_\omega F_{pw})\mathbf{h} \times (\mathbf{n} \times \mathbf{p}_s)$, where E_F is the Fermi energy. The typical amplitude is $|\mathbf{d}_s| \sim (p_s \xi)\hbar v_F \alpha / \Delta^2$ where ξ is the coherence length. To produce both the p-wave and s-wave triplets it is crucial to have $\mathbf{h} \neq 0$ so that they

are qualitatively different from those obtained beyond quasiclassical approximation due to the Edelstein effect^{56–58}. The vector field $\mathbf{d} = \mathbf{d}_p + \mathbf{d}_s$, where $\mathbf{d}_s \propto \mathbf{h} \times (\mathbf{n} \times \mathbf{E})$ is shown schematically in Fig. 2b where the configuration with $\mathbf{E} \parallel \mathbf{h} \perp \mathbf{n}$ results in $\mathbf{d} \parallel \mathbf{n}$ and the mixing s-p wave pairing so that $|\mathbf{d}(\mathbf{p})| \neq |\mathbf{d}(-\mathbf{p})|$.

B. Microscopic model

Quantitatively the action of the external electric field on the SFS junction can be described by the Usadel equation for the quasiclassical Green's function $\check{g}(\varepsilon, t, \mathbf{r})$. In the mixed (ε, t) representation it takes the form:

$$iD\hat{\partial}_{\mathbf{r}}(\check{g} \otimes \hat{\partial}_{\mathbf{r}}\check{g}) = [\hat{\tau}_3(\varepsilon - \mathbf{h}\hat{\boldsymbol{\sigma}} + \hat{\Delta}), \check{g}]_{\otimes}, \quad (4)$$

where $\hat{\tau}_i$ and $\hat{\sigma}_i$ are Pauli matrices in particle-hole and spin spaces, respectively, and $\hat{\boldsymbol{\sigma}} = (\hat{\sigma}_1, \hat{\sigma}_2, \hat{\sigma}_3)^T$. The Green's function $\check{g}(\varepsilon, t, \mathbf{r})$ is a 8×8 matrix in the direct product of particle-hole, spin and Keldysh spaces. It describes two-particle correlations and depends on "center of mass" coordinate \mathbf{r} . In addition the mixed representation means the Fourier transform $t_1 - t_2 \rightarrow \varepsilon$, but the resulting Green's function still depends on time via $t = (t_1 + t_2)/2$ because of the non-stationary character on the problem under consideration. In the mixed representation usual multiplication is replaced by the \otimes -product, which is defined as $\hat{A} \otimes \hat{B} = \exp((i/2)(\partial_{\varepsilon_A} \partial_{t_B} - \partial_{\varepsilon_B} \partial_{t_A})) \hat{A}(\varepsilon, t) \hat{B}(\varepsilon, t)$. In Eq. (4) D is the diffusion constant and $\hat{\Delta} = |\Delta(x)| \exp[i\chi(x)\hat{\tau}_3]\hat{\tau}_1$. We assume $|\Delta(x)| = 0$ in the interlayer of the Josephson junction $-d_F/2 \leq x \leq d_F/2$, while $|\Delta(x)| = \Delta$ and $\chi(x) = \mp\chi/2$ in the left (right) superconducting leads. The differential superoperator in Eq. (4) is

$$\hat{\partial}_k \check{g} = \nabla_k \check{g} - i[\alpha \hat{A}_k + \frac{e}{c} A_k \hat{\tau}_3, \check{g}]_{\otimes} \quad (5)$$

The presence of an alternating electric field $\mathbf{E}(t)$ is described by the time-dependent vector potential $\mathbf{E} = -\partial_t \mathbf{A}/c$. Rashba-type SOC in (5) is described by the SU(2) gauge field $\hat{A} = \mathbf{n} \times \hat{\boldsymbol{\sigma}}$.

We assume that the SOC is localized near FS interfaces at the lengthscale d_{so} much smaller than ξ_F , and also we assume the realistic limit $\xi_F \ll d_F \ll \xi_N$. In this case the SOC is absent in the most part of the normal metal interlayer and can be taken into account as effective boundary conditions at S/F interfaces $x = \mp d_F/2$. Note that the diffusive Eq. (4) takes into account only the s-wave superconducting correlations while the p-wave components which arise in the presence of SOC and exchange field vanish due to the averaging over the momentum direction characterising the relative orbital motion of the interacting electrons. However, the presence of spin-triplet p-wave correlations is taken into account through the effective boundary conditions for the s-wave component described below.

To derive the linear boundary conditions we assume the presence of tunnel barriers at the S/Pt interfaces allowing only for the weak proximity effect. That means the GF can be written in the simplified form $\hat{g}^{R,A} = \pm \hat{\tau}_3 + \check{f}^{R,A}$ where the anomalous part $\check{f}^{R,A} = \hat{f}_s^{R,A} + \boldsymbol{\sigma} \hat{f}_t^{R,A}$ can be written as the sum of spin-singlet $f_s^{R,A}$ and spin-triplet $\hat{f}_t^{R,A}$ components. The anomalous part is described by the linearized Usadel equation

$$\pm iD\partial_x^2 \check{f}^{R,A} = 2\varepsilon \check{f}^{R,A} - \{\mathbf{h}\hat{\boldsymbol{\sigma}}, \check{f}^{R,A}\}. \quad (6)$$

The effective boundary condition taking into account SOC in the thin layers of Pt at S/F interfaces has the form⁵⁹:

$$n_x \partial_x \check{f}_{tr}^{R,A} = \frac{2e}{c} \tilde{\alpha} \hat{\tau}_3 [(\mathbf{n} \times \hat{\boldsymbol{\sigma}}), \{\mathbf{A}(t), \check{f}_{tr}^{R,A}\}]_{\otimes}, \quad (7)$$

where $n_x = \pm 1$ for the left(right) S/F interface and $\tilde{\alpha} = \int dx \alpha(x)$ is the surface SOC strength. There are some terms, which are present in Eq. (4), but are omitted in Eq. (7). The reason is that they do not lead to the SRT \rightarrow LRT conversion and, therefore, are small in the framework of the perturbation theory.

The boundary condition for the singlet component is the usual Kupriyanov-Lukichev boundary condition⁶⁰

$$(\mathbf{n}\nabla) \hat{f}_s^{R,A} = \gamma \hat{F}_{bcs}^{R,A}, \quad (8)$$

where $\hat{F}_{bcs}^{R,A} = \mp \hat{\tau}_3 \hat{\Delta} / (\varepsilon \pm i\delta)$.

C. Long-range spin-triplet correlations in the Josephson junction

In general the solution of linearized Usadel Eq. (6) consists of the short-range and long-range modes. They decay in the ferromagnetic region at the distances of $\xi_F = \sqrt{D/\hbar}$ and $\xi_N \sim \sqrt{D/\Omega}$, respectively. Physically the long-range modes correspond to the LRTC components. In the considered setup they appear only under the action of the external electric field through the boundary conditions (7).

Solving the system of linear equations and boundary conditions we obtain the LRT in the Josephson setups Fig.1b,c. The amplitude of LRT has the form (1) characterized by the spin vector (2) with $\mathbf{n} = \mathbf{x}$ and the non-local kernel with Fourier components⁵⁹

$$K_d^{R,A}(\varepsilon, \Omega) = \pm \frac{4e\tilde{\alpha}\xi_F^2(\gamma\xi_F)|\Delta|\sin(\chi/2)\hat{\tau}_2}{d_F[(\varepsilon \pm i\delta)^2 - (\Omega/2)^2]\Omega}. \quad (9)$$

Here we consider the case of weak superconducting correlations in the F layer. Therefore, when calculating the current we can neglect non-equilibrium corrections to distribution functions and taking into account only the perturbations of the spectral functions given by Eq. (9).

D. Photo-induced Josephson current

In the JJ geometry of Fig.1 the LRT generated at the left and right SF interfaces overlap in the ferromagnetic inter-layer which results in the dependence on the Josephson phase difference in Eq. (9). The overlapping superconducting correlations can mediate the current between left and right superconducting electrodes driven by the order parameter phase difference.

In order to obtain the charge current we need to convert spin-triplet correlations into the spin-singlet ones. It is convenient to calculate the Josephson current at one of the interfaces. It can be written as⁵⁹:

$$j = \mp \frac{\sigma_F \gamma}{8e} \int d\varepsilon \text{Tr}_2 \left[\left\{ \hat{\tau}_3 \hat{F}_{bcs}^R, \hat{f}_s^R \otimes n_0(\varepsilon) \right\}_{\otimes} + \left\{ \hat{\tau}_3 \hat{F}_{bcs}^A, n_0(\varepsilon) \otimes \hat{f}_s^A \right\}_{\otimes} \right]. \quad (10)$$

The \mp sign is related to the left(right) S/F interfaces and $n_0(\varepsilon) = \tanh(\varepsilon/2T)$ is the Fermi distribution function. The singlet component of the anomalous Green's function at the interface can be found from Eq. (6) and boundary conditions Eqs. (7)-(8) and takes the form⁵⁹:

$$\hat{f}_{s,l(r)}^{R,A} = -\frac{\gamma\xi_F}{2}\hat{F}_{bcs,l(r)} \mp \frac{4e}{c}\tilde{\alpha}\xi_F\hat{\tau}_3 \sum_i e^{i\Omega_i t} \times \left([(\mathbf{A}_{\Omega_i} \times \mathbf{n}_{l(r)}) \times \sum_{a=\pm 1} \mathbf{d}(\varepsilon + \frac{a\Omega_i}{2}, t)] \mathbf{n}_h \right), \quad (11)$$

where $\mathbf{n}_h = \mathbf{h}/h$. The first term represents the zero-order singlet component in the absence of the electromagnetic field. This component corresponds to the opposite-spin pairs penetrating from the adjacent superconductor and decays rapidly into the depth of the ferromagnet. Thus it does not feel the opposite superconducting lead and does not provide the Josephson current, as it can be immediately seen from Eq. (10). On the contrary, the second term in Eq. (11) is physically provided by the LRT-singlet conversion near the given interface. It is expressed via the spin vector \mathbf{d} of the LRT, which contains contributions from the both interfaces and, therefore, provides a Josephson coupling between the interfaces.

For the case of a harmonic electromagnetic wave we get the current-phase relation (3) with the amplitudes of induced currents determined by the following characteristic scale $I_{dc}^c, I_{2\Omega}^c \sim I_0$ where

$$I_0 = -4S\sigma_F(\Delta/ed_F)(2\gamma\tilde{\alpha}\xi_F/\pi^2)(\xi e/\Omega)^2(\Delta/T)^2|E_\Omega|^2 \quad (12)$$

where we introduce the coherence length $\xi = \sqrt{D/\Delta}$ and the junction area $S = L_x L_y$. The current scale (12) is constructed from the quantities characterising physical mechanisms responsible for the formation of the LRT. It is proportional to the square of the LRT condensate wave function and, therefore, quadratic with respect to the electric field and surface SOC. While the nonzero exchange field is the third key ingredient to generate the LRT, expression

(12) does not disappear at $h \rightarrow 0$. The reason is that it is obtained in the limit of rather strong exchange field $\xi_F \ll \xi_N$ and $\gamma\xi_F < 1$.

The current magnitude I_0 can be estimated using the typical parameters of JJ with ferromagnetic interlayers⁶¹. Assuming that the junction area is $50 \times 50 \mu\text{m}^2$, $\sigma_F \sim (50 \mu\Omega \text{ cm})^{-1}$, $d_F \sim \gamma^{-1} \sim 5\xi_F$ and $D \sim 10 \text{ cm}^2/\text{s}$, $h \sim 500 \text{ K}$ so that $\xi_F \sim 3 \text{ nm}$. For the superconducting gap in Nb $\Delta \sim 10 \text{ K}$ so that the critical current is $I_0 \sim 10^{-1} (p_s \xi)^2 \tilde{\alpha}^2 \text{ A}$. Taking $\tilde{\alpha} \sim 0.1 - 1$ ^{15,62,63} we get the current $I_0 / (p_s \xi)^2 \sim 10^{-1} - 10^{-3} \text{ A}$. The condensate momentum is given by $|p_s| = 2eE_\Omega / \Omega$ and with the help of that we can estimate the critical current in terms of the incoming radiation power $P = c|E_\Omega|^2$ or the ac voltage applied to the the F interlayer. For the system shown in Fig. 1(b) this yields $(p_s \xi)^2 = P / P_c$ where $P_c = (ch/e^2)\hbar\Omega^2/\xi^2$ is the radiation power needed to speed up the Cooper pairs to the depairing velocity. Given that $\xi \approx 30 \text{ nm}$ we get $P_c \approx 10(\Omega/\text{GHz})^2 \text{ W}/\text{m}^2$. Therefore such JJ is quite sensitive to the radio-frequency and microwave irradiation. A typical cell phone at one meter distance generates microwave radiation with $\Omega \approx 3 - 4 \text{ GHz}$ and $P \sim P_c$ which induces rather large currents $I_0 \sim 10^{-1} - 10^{-3} \text{ A}$. At the same time the power sensitivity strongly decreases with the frequency rise. For the frequency corresponding to the cosmic background radiation $P_c \approx 10^6 \text{ W}/\text{m}^2$ so that the power density $P = 10^{-5} \text{ W}/\text{m}^2$ induces rather small critical current $I_0 \sim 10^{-12} - 10^{-15} \text{ A}$. Still, it is possible to induce large critical current using THz and visible light radiation sources. The 1 THz radiation with power 1 mW /mm² yields $I_0 \sim 10^{-5} - 10^{-7} \text{ A}$. Laser beam of the frequency about $\Omega \sim 10^6 \text{ GHz}$ carrying the power 1 mW focused into the spot of $1 \mu\text{m}^2$ size induces the critical current $I_0 \sim 10^{-6} - 10^{-8} \text{ A}$ which is well withing the measurable limits.

For the system shown in Fig. 1c we can find the ac current amplitude needed to reach the maximal critical current condition $p_s \xi \sim 1$. The threshold current density is given by $j \approx 10^{-9} \text{ A}/\text{cm}^2$. For $\Omega = 1 \text{ GHz}$ and conductivity $\sigma \sim (50 \mu\Omega \text{ cm})^{-1}$ such current density is generated by the voltage in the range of mV applied to the centimeter-long wire.

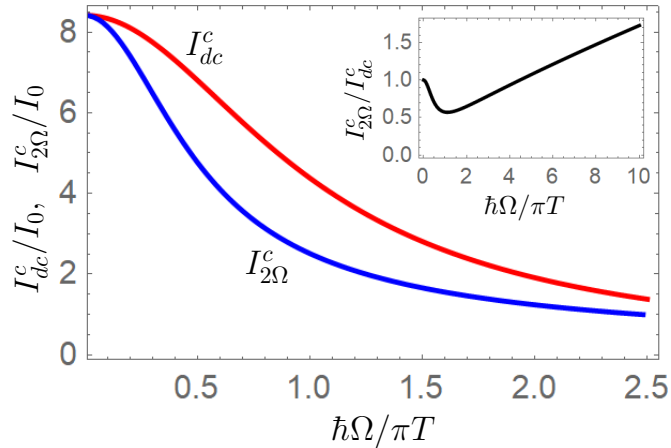


FIG. 3. **DC and double-frequency components of the critical current.** I_{dc}^c (red) and $I_{2\Omega}^c$ (blue) as functions of $\Omega/\pi T$. The currents are normalized to I_0 . Insert demonstrates the ratio $I_{2\Omega}^c/I_{dc}^c$ as a function of frequency.

Exact analytical expressions for I_{dc}^c and $I_{2\Omega}^c$ can be found in the supplementary material⁵⁹. The behavior of dc I_{dc}^c second harmonic $I_{2\Omega}^c$ components of the current in Eq. (3) as functions of the frequency $\Omega/\pi T$ is plotted in Fig. 3. It is seen that the dc component dominates at $\hbar\Omega/\pi T \lesssim 1$, what corresponds to the frequencies range up to THz range at not very low cryogenic temperatures.

It is interesting to note that the dc component of the Josephson current $I_{dc}^c < 0$. That is the junction manifests the π -junction behavior. The physical reason is that the condensate momenta generated by the alternating electric field are equal (and not opposite to each other as it takes place for the case of the condensate momenta generated by the static magnetic field) at the both S/F interfaces. Taking into account opposite signs of the interfaces normal vectors at the left and right interfaces, we obtain that the phases of the LRTs generated by the interfaces differ by $\chi + \pi$. This additional factor π gives rise to the factor $\sin \chi/2$ in Eq. (9) and makes the π -state of the Josephson junction to be energetically favorable.

E. Even Shapiro steps

The presence of the second harmonic contribution to the critical Josephson current (3) leads to the unusual IV-characteristics of the junction under irradiation. The examples are demonstrated in Fig. 4. First of all, we can see Shapiro step-like features. It is well-known that Shapiro steps can be observed at $2eV = \hbar n\Omega$ in conventional Josephson junction under periodic external perturbations: a periodic applied current or under irradiation. However, in sharp contrast to the case of the conventional Josephson junction, for the system under consideration the Shapiro steps take place at voltages $2eV = 2\hbar n\Omega$. That is, comparing with the usual JJ only the even-numbered Shapiro steps show up in the photo-active JJ. Obviously, it is a consequence of the fact that the ac component of the current oscillates with a frequency twice larger than the externally applied source. The second essential difference with the conventional case is that the value of the critical current grows with the irradiation power, as it is demonstrated by different curves in Fig. 4. This is a signature of the irradiation-induced LRT correlations.

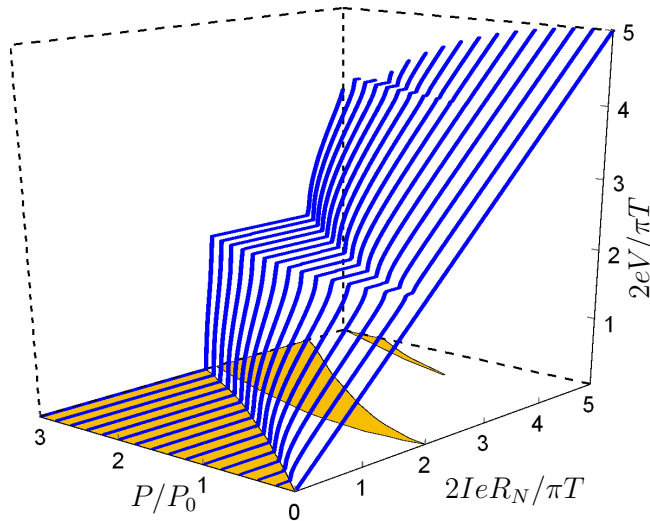


FIG. 4. **IV-characteristics of the irradiated photo-active JJ.** Different blue curves correspond to different values of the applied irradiation power at a given frequency, which is measured in units of $P_0 = 2eR_N I_{dc}^c / (\pi T)$, where R_N is the junction resistance in the normal state. $\hbar\Omega/\pi T = 1$. Shown with yellow shadings are the domains in (I, P) plane with constant voltage generated across the JJ.

F. Josephson photo-magnetic devices

Electric-field induced current across the JJ, described by Eqs. (3), (12), provides an interesting possibility to create photo-magnetic devices based on the superconducting loops with the weak links formed by the radiation-controlled JJ. We show that applying the radiation as it is shown in the schematic Fig.5 it is possible to generate spontaneous currents circulating in the loop which in turn produce a dc component of the magnetic field \mathbf{B}_{dc} .

We consider a dc SQUID with one of the branches connected by photo-active JJ and the other by the ordinary JJ with current-phase relation $I(\chi) = I_o^c \sin \chi$. Dynamics of Josephson phases χ_1 across the photo-active JJ and χ_2 across the ordinary JJ is determined by the system of coupled sine-Gordon equations⁶⁴ which is similar to the one used for the standard dc SQUID. The essentially different effects are determined by the two factors. The first one is the possibility of various parametric effects due to the time-dependent current amplitude in the photo-active JJ 3. These effects can be expected for the frequencies comparable with the eigen frequency of the superconducting loop $\omega_0 = 1/\sqrt{LC}$. Here we consider the opposite case when $\Omega \ll \omega_0$ and use the second non-trivial property of the system which is the critical current of the photo-active JJ controllable by the radiation power.

In this case we can separate the time scales corresponding to rapid oscillations and slow period-averages drift described by the coordinate $\chi = (\bar{\chi}_1, \bar{\chi}_2)$ where $\bar{\chi}_k = \Omega \int_0^{\Omega^{-1}} \chi_k dt$. We assume that the photo-induced currents are significantly small so that $\omega_{ph} \ll \Omega$, where $\omega_{ph} = \sqrt{2\pi I_{dc}^c / C\Phi_0}$ is the corresponding Josephson plasma frequency. Under this conditions we can neglect the contribution to the force of the order $(\omega_{ph}/\Omega)^2$ coming from averaging the

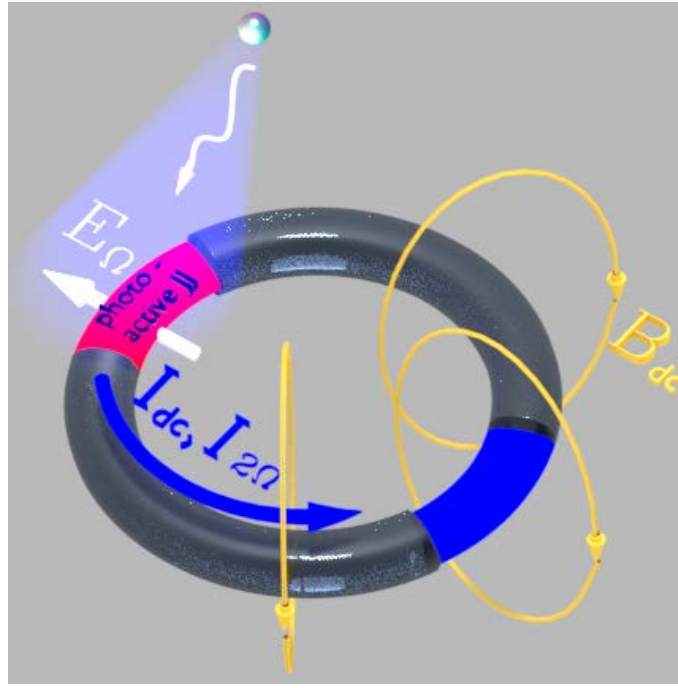


FIG. 5. **Schematic picture of the photo-magnetic SQUID.** The device consists of the photo-active Josephson junction (red weak link) and the usual JJ (blue weak link). Electric field $\mathbf{E}_\Omega e^{i\Omega t}$ from the incoming radiation switches on both dc I_{dc} and $I_{2\Omega} e^{2i\Omega t}$ components of the circulating current. The dc component produces spontaneous magnetic field \mathbf{B}_{dc} shown by yellow arrows.

second-harmonic contribution to current. Then the period-averaged phases satisfy equation

$$\partial_t^2 \chi + \gamma \partial_t \chi = -\partial_\chi U(\chi) \quad (13)$$

$$U(\chi) = \frac{\omega_0^2}{2} (\chi_1 + \chi_2)^2 - \omega_p^2 \cos \bar{\chi}_2 + \omega_{ph}^2 \cos \bar{\chi}_1 \quad (14)$$

where $\omega_0 = 1/\sqrt{LC}$ and $\gamma = 1/RC$ which are the resonant frequency and decay rate, respectively.

The system (13) can have non-trivial stable states with spontaneous dc currents circulating in the SQUID loop and generating constant magnetic field as shown schematically in Fig.5. Note that in the absence of external irradiation $\omega_{ph} = 0$ so there are no currents and phase differences are $\bar{\chi}_{1,2} = 0$. Radiation switches on the photo-active JJ $\omega_{ph} \neq 0$ and increasing gradually the radiation power we get the increase that this the zero-current state becomes unstable under the following condition

$$I_{dc}^c > \frac{\Phi_0}{2\pi} \frac{\omega_0 \omega_p}{\sqrt{\omega_0^2 + \omega_p^2}} \quad (15)$$

where $\omega_p = \sqrt{2\pi I_\pi^c / C \Phi_0}$ is the plasma frequency corresponding to the ordinary JJ. In case of the typical values $\omega_p = \omega_0 \sim 10$ GHz we get the threshold value in the r.h.s. of Eq. (15) about 10^{-6} A which is smaller than the critical currents induced by the typical THz and visible light sources according to the estimation given by Eq. (12).

Once the condition (15) is satisfied the SQUID switches to the state with spontaneous dc current I_{dc} and constant magnetic field \mathbf{B}_{dc} shown schematically in Fig.5. The photo-induced magnetic flux magnitude can be estimated as $L I_{dc}^c$. For the typical values of the SQUID loop inductance $L \approx 10^{-11}$ H and $I_{dc}^c \approx 10^{-6}$ A we get the flux of $10^{-2} \Phi_0$.

One can obtain the photo-magnetic response without any threshold for the incoming power provided the second branch of the SQUID contains the Josephson phase battery⁶⁵⁻⁶⁸ based on the JJ with shifted current-phase relation $I = I_\varphi^c \sin(\chi - \varphi_0)$ with $\varphi_0 \neq \pi n$. Such photo-magnetic element generates dc current $I_{dc} \approx I_{dc}^c \cos \varphi_0$ and the corresponding magnetic field \mathbf{B}_{dc} being exposed to any arbitrary small radiation power.

III. CONCLUSION

We have demonstrated the possibility of generating dynamical spin-triplet superconducting order which emerges under non-equilibrium conditions induced by the alternating electric field. Our proposal is based on the unusual electronic properties found in the family of quantum materials consisting of usual superconductors and ferromagnets in the presence of the interfacial Rashba-type spin-orbital coupling. Qualitatively the obtained effect arises due to the partial conversion of the p -wave triplet superconductivity, taking place in the presence of the Rashba SOC and ferromagnetism, to the s -wave odd-frequency triplet correlations. The conversion is caused by the Doppler shift of the quasiparticle spectrum induced by the non-stationary condensate motion under the action of the electric field. We provide the detailed qualitative discussion and develop the microscopic model of this mechanism. We predict the stimulation of critical current by electromagnetic radiation or by the ac voltage in Josephson junctions with interlayers hosting ferromagnetism and interfacial SOC. Such junctions also demonstrate an even-numbered sequence of Shapiro steps due to the presence of the double-frequency component in the critical current. Based on the effect of electric-field controlled spin-triplet superconductivity we propose a scheme of a Josephson transistor which can be switched by the ac current and a photo-magnetic SQUID, which generates magnetic fields under irradiation.

IV. AUTHOR CONTRIBUTIONS

All authors contributed to obtaining the results and writing the manuscript.

ACKNOWLEDGMENTS

The work of M.A.S was supported by the Academy of Finland (Project No. 297439) and Russian Science Foundation, Grant No. 19-19-00594. The work of I.V.B and A.M.B has been carried out within the state task of ISSP RAS with the support by RFBR grants 19-02-00466, 18-52-45011 and 18-02-00318. I.V.B. also acknowledges the financial support by Foundation for the Advancement of Theoretical Physics and Mathematics BASIS.

V. METHODS

All the microscopic calculations are performed in the framework of the Green's function approach. The problem under consideration is essentially nonequilibrium, therefore we make use of Keldysh technique for the Green's function calculation⁶⁹. The essence of this technique is that the Green's function consists of the retarded, advanced and Keldysh parts, which are combined to the 2×2 matrix structure in the Keldysh space. It allows for compact taking into account nonequilibrium quasiparticle distribution and explicit dependence of the Green's function on time. In this technique the Green's function is a 8×8 matrix in the direct product of particle-hole (accounting for superconductivity), spin and Keldysh spaces. It describes the two-particle correlation functions and therefore, in general, depends on two times $t_{1,2}$ and two coordinates $\mathbf{r}_{1,2}$. In our work this matrix Green's function is calculated in the framework of the quasiclassical theory of superconductivity. The quasiclassical approximation used in order to derive Eq. (4) means averaging out the relative coordinate so that the GF depends of the single "center of mass" coordinate. In addition, the mixed representation means the Fourier transform $t_1 - t_2 \rightarrow \varepsilon$, but the resulting Green's function still depends on time via $t = (t_1 + t_2)/2$ because of the non-stationary character on the problem under consideration. Usage of the quasiclassical equation in the form of the Usadel equation⁷⁰, expressed by Eq. (4), also means that we consider the diffusive limit corresponding to $l \ll \xi$, where l is the mean free path. Under this condition the quasiclassical Green's function is effectively isotropic in the leading approximation and, therefore, the direction of the quasiparticle trajectory does not enter Eq. (4). Observables can be calculated via the quasiclassical Green's function. In the present work we focus on the Josephson current and the details of the corresponding calculation are provided in the supplementary material⁵⁹.

VI. COMPETING INTERESTS

The authors declare no competing interests.

VII. DATA AVAILABILITY

No datasets were generated or analysed during the current study.

-
- ¹ T. Clark, R. Prance, and A. Grassie, *Journal of Applied Physics* **51**, 2736 (1980).
 - ² K. K. Likharev and V. K. Semenov, *IEEE Transactions on Applied Superconductivity* **1**, 3 (1991).
 - ³ T. W. Larsen, K. D. Petersson, F. Kuemmeth, T. S. Jespersen, P. Krogstrup, J. Nygård, and C. M. Marcus, *Physical review letters* **115**, 127001 (2015).
 - ⁴ L. Casparis, T. Larsen, M. Olsen, F. Kuemmeth, P. Krogstrup, J. Nygård, K. Petersson, and C. Marcus, *Physical review letters* **116**, 150505 (2016).
 - ⁵ A. Volkov, *Physical review letters* **74**, 4730 (1995).
 - ⁶ A. Morpurgo, T. Klapwijk, and B. Van Wees, *Applied physics letters* **72**, 966 (1998).
 - ⁷ J. Baselmans, A. Morpurgo, B. Van Wees, and T. Klapwijk, *Nature* **397**, 43 (1999).
 - ⁸ J. Huang, F. Pierre, T. T. Heikkilä, F. K. Wilhelm, and N. O. Birge, *Physical Review B* **66**, 020507 (2002).
 - ⁹ F. Paolucci, F. Vischi, G. De Simoni, C. Guarcello, P. Solinas, and F. Giazotto, *Nano letters* **19**, 6263 (2019).
 - ¹⁰ G. De Simoni, F. Paolucci, P. Solinas, E. Strambini, and F. Giazotto, *Nature nanotechnology* **13**, 802 (2018).
 - ¹¹ Y.-J. Doh, J. A. van Dam, A. L. Roest, E. P. Bakkers, L. P. Kouwenhoven, and S. De Franceschi, *science* **309**, 272 (2005).
 - ¹² S. Abay, D. Persson, H. Nilsson, F. Wu, H. Xu, M. Fogelström, V. Shumeiko, and P. Delsing, *Physical Review B* **89**, 214508 (2014).
 - ¹³ J. A. Van Dam, Y. V. Nazarov, E. P. Bakkers, S. De Franceschi, and L. P. Kouwenhoven, *Nature* **442**, 667 (2006).
 - ¹⁴ D. Szombati, S. Nadj-Perge, D. Car, S. Plissard, E. Bakkers, and L. Kouwenhoven, *Nature Physics* **12**, 568 (2016).
 - ¹⁵ C. R. Ast, J. Henk, A. Ernst, L. Moreschini, M. C. Falub, D. Pacilé, P. Bruno, K. Kern, and M. Gioni, *Physical Review Letters* **98**, 186807 (2007).
 - ¹⁶ G. Bihlmayer, Y. M. Koroteev, P. Echenique, E. Chulkov, and S. Blügel, *surface science* **600**, 3888 (2006).
 - ¹⁷ A. Manchon, H. C. Koo, J. Nitta, S. Frolov, and R. Duine, *Nature materials* **14**, 871 (2015).
 - ¹⁸ N. H. Lindner, G. Refael, and V. Galitski, *Nature Physics* **7**, 490 (2011).
 - ¹⁹ F. Wilczek, *Physical review letters* **111**, 250402 (2013).
 - ²⁰ N. Y. Yao, A. C. Potter, I.-D. Potirniche, and A. Vishwanath, *Physical review letters* **118**, 030401 (2017).
 - ²¹ S. Autti, V. Eltsov, and G. Volovik, *Physical review letters* **120**, 215301 (2018).
 - ²² C. Triola, A. Pertsova, R. S. Markiewicz, and A. V. Balatsky, *Physical Review B* **95**, 205410 (2017).
 - ²³ D. Fausti, R. Tobey, N. Dean, S. Kaiser, A. Dienst, M. C. Hoffmann, S. Pyon, T. Takayama, H. Takagi, and A. Cavalleri, *science* **331**, 189 (2011).
 - ²⁴ M. Claassen, D. M. Kennes, M. Zingl, M. A. Sentef, and A. Rubio, *Nature Physics* **15**, 766 (2019).
 - ²⁵ A. V. Balatsky, P. O. Sukhachov, and S. Bandyopadhyay, *Annalen der Physik* **532**, 1900529 (2020).
 - ²⁶ F. Bergeret, A. Volkov, and K. Efetov, *Rev. Mod. Phys.* **77**, 1321 (2005).
 - ²⁷ A. J. Leggett, *Reviews of Modern Physics* **47**, 331 (1975).
 - ²⁸ M. Eschrig and T. Löfwander, *Nature Physics* **4**, 138 (2008).
 - ²⁹ J. W. A. Robinson, G. B. Halsz, A. I. Buzdin, and M. G. Blamire, *Phys. Rev. Lett.* **104**, 207001 (2010).
 - ³⁰ J. W. A. Robinson, J. D. S. Witt, and M. G. Blamire, *Science* **329**, 59 (2010).
 - ³¹ K. Lahabi, M. Amundsen, J. A. Ouassou, E. Beukers, M. Pleijster, J. Linder, P. Alkemade, and J. Aarts, *Nature communications* **8**, 2056 (2017).
 - ³² F. Konschelle, I. V. Tokatly, and F. S. Bergeret, *Phys. Rev. B* **92**, 125443 (2015).
 - ³³ F. Bergeret and I. Tokatly, *Phys. Rev. Lett.* **110**, 117003 (2013).
 - ³⁴ F. Bergeret and I. Tokatly, *Phys. Rev. B* **89**, 134517 (2014).
 - ³⁵ I. V. Tokatly, *Phys. Rev. B* **96**, 060502 (2017).
 - ³⁶ X. Montiel and M. Eschrig, *Phys. Rev. B* **98**, 104513 (2018).
 - ³⁷ J. Linder and J. W. A. Robinson, *Nat Phys* **11**, 307 (2015).
 - ³⁸ M. Eschrig, *Reports on Progress in Physics* **78**, 104501 (2015).
 - ³⁹ S. Vaitiekėnas, Y. Liu, P. Krogstrup, and C. Marcus, *arXiv preprint arXiv:2004.02226* (2020).
 - ⁴⁰ S. Manna, P. Wei, Y. Xie, K. T. Law, P. A. Lee, and J. S. Moodera, *Proceedings of the National Academy of Sciences* **117**, 8775 (2020).
 - ⁴¹ J.-X. Zhu, Z. Nussinov, A. Shnirman, and A. V. Balatsky, *Physical review letters* **92**, 107001 (2004).
 - ⁴² M. Houzet, *Physical review letters* **101**, 057009 (2008).
 - ⁴³ A. F. Volkov and K. B. Efetov, *Phys. Rev. Lett.* **103**, 037003 (2009).
 - ⁴⁴ T. Yokoyama and Y. Tserkovnyak, *Physical Review B* **80**, 104416 (2009).
 - ⁴⁵ J. Linder and A. V. Balatsky, *Reviews of Modern Physics* **91**, 045005 (2019).
 - ⁴⁶ G. Aeppli, A. V. Balatsky, H. M. Rønnow, and N. A. Spaldin, *Nature Reviews Materials* , 1 (2020).
 - ⁴⁷ L. Stojchevska, I. Vaskivskiy, T. Mertelj, P. Kusar, D. Svetin, S. Brazovskii, and D. Mihailovic, *Science* **344**, 177 (2014).
 - ⁴⁸ V. Berezinskii, *Jetp Lett* **20**, 287 (1974).
 - ⁴⁹ D. Belitz and T. Kirkpatrick, *Physical Review B* **46**, 8393 (1992).

- ⁵⁰ A. Balatsky and E. Abrahams, *Physical Review B* **45**, 13125 (1992).
- ⁵¹ E. Abrahams, A. Balatsky, D. Scalapino, and J. Schrieffer, *Physical Review B* **52**, 1271 (1995).
- ⁵² P. Coleman, E. Miranda, and A. Tsvelik, *Physical Review B* **49**, 8955 (1994).
- ⁵³ A. M. Black-Schaffer and A. V. Balatsky, *Physical Review B* **86**, 144506 (2012).
- ⁵⁴ W. V. Budzinski, M. P. Garfunkel, and R. W. Markley, *Phys. Rev. B* **7**, 1001 (1973).
- ⁵⁵ A. Kohen, T. Proslir, T. Cren, Y. Noat, W. Sacks, H. Berger, and D. Roditchev, *Physical review letters* **97**, 027001 (2006).
- ⁵⁶ C. R. Reeg and D. L. Maslov, *Phys. Rev. B* **92**, 134512 (2015).
- ⁵⁷ I. V. Bobkova and A. M. Bobkov, *Phys. Rev. B* **95**, 184518 (2017).
- ⁵⁸ F. Korschelle, I. V. Tokatly, and F. S. Bergeret, *Phys. Rev. B* **94**, 014515 (2016).
- ⁵⁹ For details of the derivation see Supplementary material at.
- ⁶⁰ M. Y. Kuprianov and V. F. Lukichev, *JETP* **1163**, 78 (1988), [*Zh. Eksp. Teor. Fiz.* **94**, 139 (1988)].
- ⁶¹ Y. V. Fominov, A. Volkov, and K. Efetov, *Physical Review B* **75**, 104509 (2007).
- ⁶² S.-T. Lo, S.-W. Lin, Y.-T. Wang, S.-D. Lin, and C.-T. Liang, *Scientific reports* **4**, 5438 (2014).
- ⁶³ N. Banerjee, J. A. Ouassou, Y. Zhu, N. Stelmashenko, J. Linder, and M. G. Blamire, *Physical Review B* **97**, 184521 (2018).
- ⁶⁴ A. Barone and G. Paterno, *Physics and applications of the Josephson effect* (Wiley, 1982).
- ⁶⁵ A. Buzdin, *Phys. Rev. Lett.* **101**, 107005 (2008).
- ⁶⁶ D. B. Szombati, S. Nadj-Perge, D. Car, S. R. Plissard, E. P. A. M. Bakkers, and L. P. Kouwenhoven, *Nature Physics* **12**, 568 EP (2016).
- ⁶⁷ A. Assouline, C. Feuillet-Palma, N. Bergeal, T. Zhang, A. Mottaghizadeh, A. Zimmers, E. Lhuillier, M. Eddrie, P. Atkinson, M. Aprili, *et al.*, *Nature communications* **10**, 1 (2019).
- ⁶⁸ E. Strambini, A. Iorio, O. Durante, R. Citro, C. Sanz-Fernández, C. Guarcello, I. V. Tokatly, A. Braggio, M. Rocci, N. Ligato, *et al.*, *Nature Nanotechnology* , 1 (2020).
- ⁶⁹ J. Rammer and H. Smith, *Rev. Mod. Phys.* **58**, 323 (1986).
- ⁷⁰ K. Usadel, *Phys. Rev. Lett.* **25**, 507 (1977).